



RESEARCH LETTER

10.1002/2017GL076640

Key Points:

- Against expectation, bulk entrainment rate increases when convection aggregates in convection-permitting RCE simulations
- Aggregated updrafts have high bulk entrainment rates because they are densely packed, generating a lot of shear and turbulence
- Aggregated updrafts are protected by a moist shell and therefore experience less buoyancy reduction through entrainment

Correspondence to:

T. Becker,
tobias.becker@mpimet.mpg.de

Citation:

Becker, T., Bretherton, C. S., Hohenegger, C., & Stevens, B. (2018). Estimating bulk entrainment with unaggregated and aggregated convection. *Geophysical Research Letters*, 45, 455–462. <https://doi.org/10.1002/2017GL076640>

Received 22 SEP 2017

Accepted 21 DEC 2017

Accepted article online 27 DEC 2017

Published online 15 JAN 2018

Estimating Bulk Entrainment With Unaggregated and Aggregated Convection

Tobias Becker¹ , Christopher S. Bretherton² , Cathy Hohenegger¹ , and Bjorn Stevens¹ 

¹Max Planck Institute for Meteorology, Hamburg, Germany, ²Departments of Atmospheric Science and Applied Mathematics, University of Washington, Seattle, WA, USA

Abstract To investigate how entrainment is influenced by convective organization, we use the ICON (ICOsahedral Nonhydrostatic) model in a radiative–convective equilibrium framework, with a 1 km spatial grid mesh covering a 600 by 520 km² domain. We analyze two simulations, with unaggregated and aggregated convection, and find that, in the lower free troposphere, the bulk entrainment rate increases when convection aggregates. The increase of entrainment rate with aggregation is caused by a strong increase of turbulence in the close environment of updrafts, masking other effects like the increase of updraft size and of static stability with aggregation. Even though entrainment rate increases with aggregation, updraft buoyancy reduction through entrainment decreases because aggregated updrafts are protected by a moist shell. Parameterizations that wish to represent mesoscale convective organization would need to model this moist shell.

1. Introduction

Many general circulation model (GCM) studies have identified the entrainment parameter of the convection scheme as being exceptionally important for the climate and climate change simulated by the models (e.g., Klocke et al., 2011; Knight et al., 2007; Sherwood et al., 2014; Tomassini et al., 2015), as well as for the organization of convection (e.g., Arnold & Randall, 2015; Becker et al., 2017; Oueslati & Bellon, 2013; Tompkins & Semie, 2017). The concept of entrainment, as it appears in many models, arises from a bulk ansatz whereby convection is modeled by a mass flux whose properties are distinct from the environment through which it rises. Entrainment alters both the convection and its environment, affecting, for instance, the vertical energy transport, static stability, and the cloud profile, as well as the overturning circulation and the organization of convection in the tropics. Although there have already been many attempts to estimate bulk entrainment rate, both from observations (e.g., Esbensen, 1978; Yanai et al., 1973) and, more recently, from convection-permitting models (e.g., Lu et al., 2016; Romps, 2010; Siebesma & Cuijpers, 1995; Siebesma et al., 2003; Zhang et al., 2016); (review article by de Rooy et al., 2013), questions arise as to whether, for a cumulus layer of a given depth, the bulk entrainment rate shows a clear dependence on convective organization.

The bulk ansatz, together with a too small parameter space, results in what some authors have called the entrainment dilemma in convective parameterizations: if the entrainment parameter is large, convection is too much suppressed, causing an accumulation of instability, and if the entrainment parameter is small, convection occurs too readily, causing a poor distribution of convection in space and time, associated with too little variability. Mapes and Neale (2011) coined this phrase and hypothesized that it could be solved by incorporating convective organization as a new prognostic variable in the convection scheme, which acts as a throttle on the bulk entrainment parameter. When convection organizes, entrainment rate is believed to decrease because entrainment rate is assumed to scale with the inverse of the largest eddy sizes in the updraft (Morton et al., 1966; Turner, 1963; Siebesma, 1996), and the size of the convective updrafts increases with organization (e.g., Mapes & Neale, 2011). When convection organizes into an aggregated cluster, entrainment is also believed to have less impact on updraft buoyancy because the spacing of updrafts reduces, moistening the local environment (e.g., Feng et al., 2015; Mapes & Neale, 2011). Despite these hypotheses, the effect of convective organization on entrainment has not yet been systematically investigated.

In this study, we test whether convective organization—in the form of convective aggregation—results in the hypothesized decrease of entrainment rate and in the hypothesized decrease of updraft buoyancy reduction through entrainment. We compare bulk entrainment rate estimates for deep convection in two

convection-permitting simulations, one with unaggregated and one with aggregated convection, using the ICON model in a radiative-convective equilibrium (RCE) framework.

2. Methods

ICON (ICOsahedral Nonhydrostatic) is a unified modeling system developed jointly by the Max Planck Institute for Meteorology and the German Weather Service for global numerical weather prediction and climate studies (Zängl et al., 2015). We use its large-eddy model (ICON-LEM), developed by Dipankar et al. (2015) and evaluated in simulations over Germany by Heinze et al. (2017). Our RCE setup consists of an inertial (nonrotating) frame of reference, a prescribed SST of 300 K, and spatially homogeneous but diurnally varying (solar zenith angle: 0° , solar constant: 1069.3 W m^{-2}) insolation. Analyzing convection and how it self-aggregates in a convection-permitting RCE setup has a long tradition (e.g., Bretherton et al., 2005; Tompkins & Craig, 1998), and for the purposes of our study, the RCE setup has the advantage that the degree of convective aggregation can vary strongly, from totally unaggregated convection with a popcorn-like appearance to completely aggregated convection that organizes in a cluster.

To resolve deep convection, we analyze two simulations with 1 km grid spacing. Both simulations share an identical simulation setup, except for different initial conditions: the first simulation is initialized from unaggregated conditions, and convection stays unaggregated throughout the simulation, while the second simulation is started from fully aggregated conditions, and convection stays fully aggregated in a horizontally isotropic cluster. More precisely, the first simulation is initialized with horizontally homogeneous vertical profiles of temperature and specific humidity that stem from a small-domain simulation with unaggregated convection. The second simulation is started from day 90 of a simulation with 3 km grid spacing, which was initialized from the same initial conditions as the first simulation, but starts to self-aggregate after 30 days and is fully self-aggregated after 60 days.

We initially planned to run our two simulations for 60 days but extended the first simulation to 90 days to be sure that it does not start to self-aggregate. Some weak heterogeneities emerged, which visualize in Figure 1 as a vertically oriented swath of maximum precipitation around $x = 120 \text{ km}$. However, these weak heterogeneities have proved insufficient for self-aggregation to kick in. In line with Muller and Bony (2015), the absence of self-aggregation at high resolution can be explained with a weaker shallow overturning circulation due to less longwave cooling from low clouds in the subsidence region. This mechanism does not affect the process that we analyze in this study—entrainment—and how it depends on convective aggregation.

Except for the already discussed differences in the initial conditions, the two simulations share exactly the same physics and boundary conditions. They are run on 64 vertical levels, with a model top at 27 km. In the horizontal, the model spans a 600 by 520 km^2 domain with periodic boundary conditions. For parameterizations, we use classical Smagorinsky diffusion with the modifications by Lilly (1962) to account for thermal stratification, the two-moment mixed-phase bulk microphysical parameterization of Seifert and Beheng (2006), and the Rapid Radiation Transfer Model for radiation (Mlawer et al., 1997). For clouds and convection, no parameterizations are used.

To quantify bulk entrainment rate, previous studies have used different tracers, for example, a “purity tracer” (Romps, 2010) or a “radioactive tracer” (Couvreur et al., 2010; Romps & Kuang, 2011). Here we quantify bulk entrainment rate with a radioactive tracer that is injected in the lowest model level, which ensures that updrafts have higher tracer concentrations than their environment. In the atmosphere, the radioactive tracer decays with an e -folding time scale of 4 days. With this decay time scale, tracer decay within the updraft is at most 2% of the change induced by entrainment, as calculated by dividing the ascent-decay time scale by the dilution time scale. In addition, with this decay time scale, the difference between updraft and environmental tracer concentration is high enough (see section 3.1 for details) to get reliable bulk entrainment rate estimates.

Bulk entrainment rate is analyzed using three-hourly output from the last 30 days of each simulation. Grid points are defined to be convective updraft grid points if the upward velocity exceeds 1 m s^{-1} and if the sum of liquid and ice condensate exceeds 0.01 g kg^{-1} . The environmental tracer concentration is calculated by averaging over all nonupdraft grid points on the same model level within a 10 km neighborhood of every updraft grid point. To make this analysis more computationally tractable, the environmental tracer concentration is calculated after nearest-neighbor remapping (effectively subsampling) to a 3 km grid. The updraft (ϕ_u) and environmental (ϕ_e) tracer concentrations are averaged over space and time, whereby an updraft mass flux

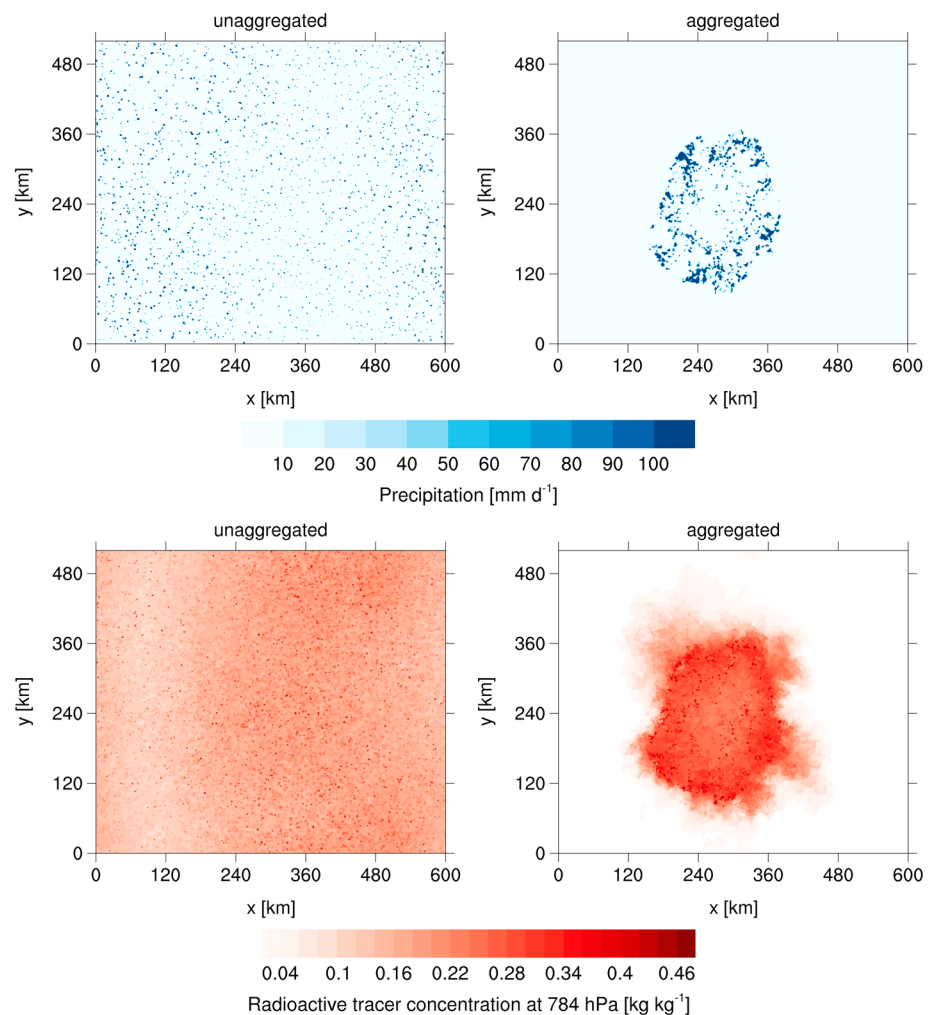


Figure 1. (top row) Snapshots of precipitation (3 h mean) and (bottom row) radioactive tracer concentration (instantaneous) with unaggregated and aggregated convection at 784 hPa (2,196 m), representing the lower troposphere.

weighting (Hohenegger & Bretherton, 2011) is applied for the updraft tracer concentration ($\hat{\phi}_u$), to emphasize the importance of strong updrafts. After the weighted averaging, the bulk entrainment rate is estimated following Betts (1975):

$$\epsilon = \frac{-\partial_z \hat{\phi}_u}{\hat{\phi}_u - \phi_e} \tag{1}$$

3. Results

3.1. Aggregated and Unaggregated Convection in ICON-LEM

Snapshots of the two simulations with unaggregated and aggregated convection (Figure 1) illustrate that in the lower troposphere (784 hPa), precipitating and nonprecipitating regions can be well separated with the radioactive tracer. Radioactive tracer concentrations, set to 1.0 at the surface, are about 0.4 or more in the convective updrafts. Outside convective updrafts, the tracer concentration strongly depends on the degree of aggregation. In unaggregated states, the tracer is homogeneously distributed, with tracer concentrations of 0.1 to 0.2. In aggregated states, nonupdraft grid points within the convective cluster have larger tracer concentrations (about 0.3), but outside the convective cluster, tracer concentrations are almost zero.

The strongest updrafts, associated with the highest tracer concentration, occur at the edges of the aggregated cluster of convection, in agreement with Hohenegger and Stevens (2016). The reason is that these locations are very favorable for convection: moisture convergence in the boundary layer is high, and the

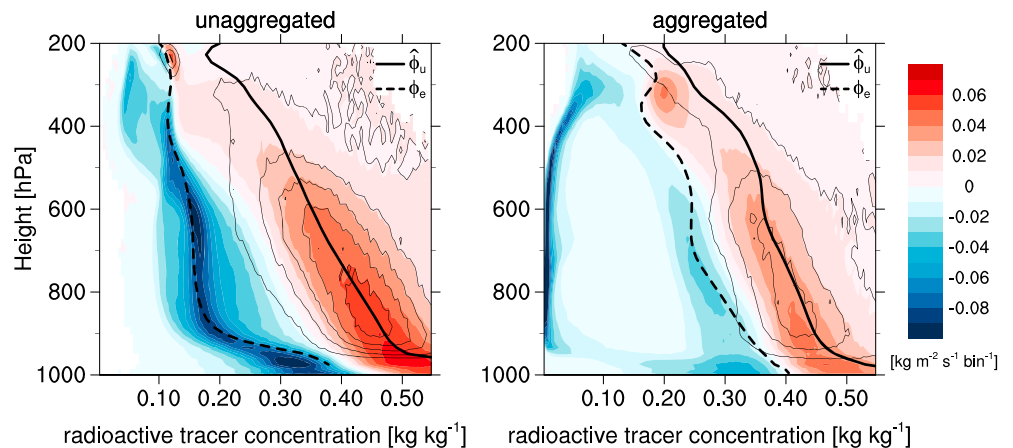


Figure 2. Vertical mass flux in a height-tracer concentration space (tracer concentration bin width: 0.005 kg kg^{-1}), both with unaggregated and aggregated convection, averaged over the last 30 days of each simulation. Updraft mass flux ($w > 1 \text{ m s}^{-1}$, saturated) is represented by black contour lines, with $0.01 \text{ kg m}^{-2} \text{ s}^{-1} \text{ bin}^{-1}$ intervals, starting at $0.01 \text{ kg m}^{-2} \text{ s}^{-1} \text{ bin}^{-1}$. Mass flux is defined as the product of density, vertical velocity, and horizontal area fraction. The solid and dashed thick black lines show the mean vertical profiles of the radioactive tracer in the updraft (mass flux weighted, $\hat{\phi}_u$) and in the local environment (10 km neighborhood, $\hat{\phi}_e$), respectively.

free troposphere is relatively moist. Outside the aggregated convective cluster, the dry troposphere suppresses convection. The aggregated convective cluster is very stationary, which implies that the large-scale overturning circulation is well-organized.

3.2. Estimating the Bulk Entrainment Rate

The profiles of vertical mass flux and updraft mass flux in Figure 2 show that, both with aggregated and unaggregated convection, most updrafts form at or below 900 hPa and dissipate at the freezing level (at 600 hPa) or at the tropopause (at 200 hPa). In layers where a lot of updrafts form or detrain, the bulk ansatz reaches its limits because the change of the bulk mean value with height does not necessarily represent the individual updrafts anymore. With aggregated convection, most of the updrafts that fail to penetrate further at the freezing level have small tracer concentrations (see inflection of solid black line in Figure 2), probably because those updrafts are too weak to undergo the transition to ice cloud thermodynamics. Because only the strong updrafts with high tracer concentrations survive, the bulk entrainment rate estimate is too small just above the freezing level. With unaggregated convection, the bulk ansatz produces reliable results up to the 300 hPa level because updraft dissipation is mostly independent of tracer concentration. Within a 10 km neighborhood around each updraft, environmental tracer concentrations are, in the unaggregated state, close to the

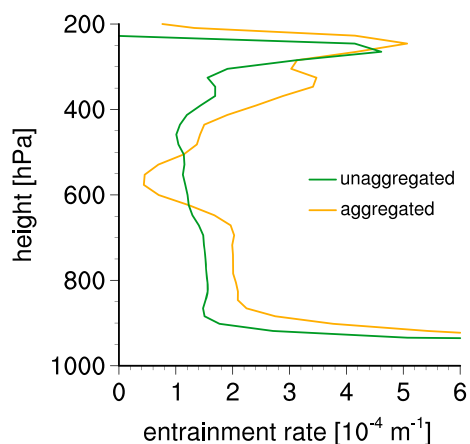


Figure 3. Bulk entrainment rate for unaggregated and aggregated convection, calculated with the radioactive tracer. For the environmental tracer concentration, a 10 km neighborhood is considered around each updraft grid point.

mean tracer concentration in the subsidence region. In the aggregated state, however, tracer concentrations are substantially higher close to the updraft than in the large-scale environment, in agreement with Figure 1.

Thus, both with unaggregated and aggregated convection, the bulk ansatz works well between 900 and 600 hPa. In line with this, bulk entrainment rate estimates are almost constant with height between 880 and 680 hPa (Figure 3). Surprisingly, given the literature cited above, the vertically averaged (880 to 680 hPa) bulk entrainment rate estimate is in aggregated conditions 40% higher than in unaggregated conditions (Table 1).

Using frozen moist static energy as tracer instead of the radioactive tracer leads to almost the same result. Over the same height range, the bulk entrainment rate is larger for aggregated ($2.2 \times 10^{-4} \text{ m}^{-1}$) than for unaggregated convection ($1.7 \times 10^{-4} \text{ m}^{-1}$). When considering values within a 30 km instead of a 10 km neighborhood around each updraft, $\hat{\phi}_u - \hat{\phi}_e$ increases in case of aggregated convection, reducing the bulk entrainment rate estimate (equation (1)), but the bulk entrainment rate estimate is still 27% higher than in case of unaggregated convection. Thus, the finding that bulk entrainment rate increases with aggregation is robust across a wide range of updraft neighborhood sizes. This is confirmed

Table 1

Vertical Averages Between 680 and 880 hPa of Entrainment Rate (ϵ), of Domain-Mean Virtual Potential Temperature Change With Height ($\partial_z \Theta_v$), of Updraft Vertical Velocity (w_u), of Specific Humidity Difference Between Updraft and 10 km Neighborhood ($q_{v,u} - q_{v,e}$), of Updraft Moist Static Energy Reduction With Height (Mass Flux Weighted, $-\partial_z \hat{h}_u$), and of Updraft Buoyancy Reduction Through Entrainment, Calculated According to Equation (4), Considering the 10 km Neighborhood for $q_{v,e}$ (B_{red})

	ϵ (10^{-4} m^{-1})	$\partial_z \Theta_v$ (K km^{-1})	w_u (m s^{-1})	$q_{v,u} - q_{v,e}$ (g kg^{-1})	$-\partial_z \hat{h}_u$ ($\text{J kg}^{-1} \text{ m}^{-1}$)	B_{red} ($\text{J kg}^{-1} \text{ m}^{-1}$)
Unaggregated	1.52	4.31	3.30	2.51	1.32	0.95
Aggregated	2.07	4.93	2.19	1.34	0.95	0.69

when comparing, for the aggregated cluster of convection, bulk entrainment rate estimates in the cluster's inner region (within a 90 km neighborhood around the center of the cluster, defined as the point where water vapor path maximizes, averaged over a 150 km neighborhood) and at its edges (outside the inner region). In the inner region of the aggregated cluster, bulk entrainment rate estimates are higher (inner region: $2.2 \times 10^{-4} \text{ m}^{-1}$, edge region: $1.9 \times 10^{-4} \text{ m}^{-1}$), even though the inner region has a more homogeneous environment, and thus the size of the considered updraft neighborhood is less relevant.

In the simulation run on a 3 km grid, which was used to initialize the 1 km simulation with aggregated convection, the bulk entrainment rate estimate is rather independent of aggregation, or, if anything, its increase with aggregation is small. This suggests that the increase of entrainment rate with aggregation is not an artifact of underresolved convection (Bryan et al., 2003). There seems to be some resolution dependence, but to the extent that no new process emerges at higher resolution, these results suggest that the increase of entrainment rate with aggregation will become, if anything, more pronounced with increasing resolution.

3.3. Why Does the Bulk Entrainment Rate Increase With Aggregation?

To find out why bulk entrainment rate increases with aggregation, we analyzed a number of different processes that are known to affect entrainment rate: updraft size, static stability, updraft velocity, organized entrainment, and turbulence near the updrafts.

In agreement with conventional wisdom (see also Mapes & Neale, 2011), updraft size increases when convection aggregates. At 700 hPa, the mean horizontal updraft extent is 1.9 km^2 for unaggregated convection and 3.6 km^2 for aggregated convection. As entrainment rate is, in the absence of other processes, inversely proportional to updraft size (e.g., Khairoutdinov & Randall, 2006; Kuang & Bretherton, 2006), entrainment rate would decrease when aggregating. Domain mean static stability increases with aggregation (see $\partial_z \Theta_v$ in Table 1), which would also tend to decrease the entrainment rate by suppressing small-scale turbulence. A countervailing effect is that, because of the higher stability, updrafts themselves also have smaller vertical velocities when aggregated (Table 1). This gives the updrafts on the one hand more time to mix but on the other hand induces less organized entrainment related to the convergence of mass. Organized entrainment might well be significantly larger in case of aggregated convection because it is accompanied by a more organized large-scale overturning circulation. However, the large-scale flow converges into the updraft grid columns almost entirely below 900 hPa. Directly above, the large-scale flow diverges, forming a shallow overturning circulation. Though the flow converges into the aggregated updrafts above that, between 680 and 780 hPa, the average horizontal velocity toward an updraft grid point in a 3 km radius around it is very small, only about 0.035 m s^{-1} . Thus, the increase of entrainment rate with aggregation cannot be attributed to organized entrainment.

The only analyzed quantity that is consistent with an increase of entrainment rate with aggregation is resolved small-scale turbulence in the close environment of the updrafts. Within a 10 km neighborhood, 2.1% of the grid points around an updraft are updraft grid points in case of unaggregated convection, and 5.6% in case of aggregated convection, averaged over 680 to 880 hPa. Thus, aggregated updrafts are more densely packed, and with their respective inflows, outflows, and downdrafts, they generate a lot of shear and turbulence. We quantify turbulence with a measure of horizontal turbulence kinetic energy (Υ), which we calculate from cross sections in x direction of u velocity (u) in the nonupdraft environment of each individual updraft grid point:

$$\Upsilon(x) = \overline{u^*(x)^2} - \overline{u^*(x)}^2, \quad (2)$$

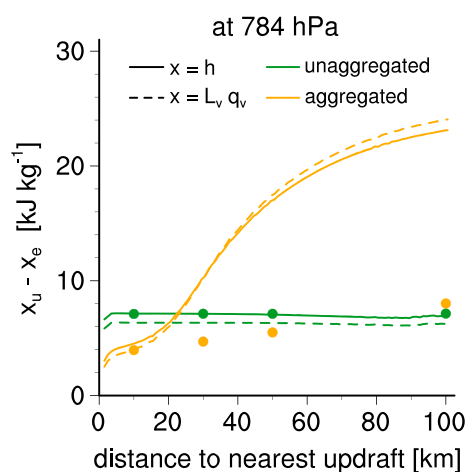


Figure 4. Difference in moist static energy and vapor energy between updraft and environment at 784 hPa (2,196 m), representing the lower troposphere. While for the updraft the bulk mean value is considered, the environmental value is sorted by the minimum distance to the closest updraft grid point. Closed circles show the difference in moist static energy between updraft and environment as well, but for the environment, they consider the bulk mean value within the respective neighborhood, calculated in analogy to ϕ_e .

where

$$u^*(x) = u(x_0 - x) - u(x_0 + x). \quad (3)$$

The average is taken over all updraft grid points in space and time; x_0 is the location of the updraft grid point, and x is the distance to the updraft. Thus, the first term in equation (2) is the mean kinetic energy in x space, the second term is the kinetic energy of the mean flow in x space, and equation (3) serves for removing transient motion from u (by mirroring the field). Averaged over 680 to 880 hPa, the estimated horizontal turbulence kinetic energy in a 3 km radius around each updraft, $\Upsilon(3 \text{ km})$, is 0.11 J kg^{-1} when unaggregated, but 0.65 J kg^{-1} when aggregated, so $\Upsilon(3 \text{ km})$ has increased sixfold.

Bulk entrainment rate estimates are highest in the inner region of the aggregated cluster, as mentioned in the last section. $\Upsilon(3 \text{ km})$ is 23% smaller in the inner region of the convective cluster than at its edges. This seems to refute the idea that changes in Υ dominate changes in entrainment rate. However, the bulk entrainment rate might be underestimated in the edge region. In the edge region, there are often dry regions with very small radioactive tracer concentrations within the considered environmental 10 km neighborhood. If air from the dry regions does not actually get entrained, the bulk entrainment rate will be underestimated (according to equation (1)).

3.4. How Does Entrainment Affect Updraft Buoyancy?

The higher entrainment rate in case of aggregated convection does not necessarily imply that updraft buoyancy decreases more with height. The efficiency of entrainment in reducing updraft buoyancy (B_{red}) can be estimated directly, from how updraft moist static energy changes with height in the lower troposphere ($-\partial_z \hat{h}_u$), or indirectly, from the saturation deficit of the environment ($q_{v,e}$) relative to the updraft ($q_{v,u}$)

$$B_{\text{red}} = \epsilon(q_{v,u} - q_{v,e})L_v, \quad (4)$$

where L_v is the enthalpy of vaporization. Both the direct and indirect approaches lead to similar results: averaged over 680 to 880 hPa, updraft buoyancy reduction through entrainment decreases by 28% when convection aggregates (Table 1), despite higher entrainment rates. This can be understood by comparing how the moist static energy deficit of the environmental air relative to the updraft ($h_u - h_e$) depends on the distance to the closest updraft grid point in unaggregated and aggregated conditions. Figure 4 shows that, on the 784 hPa level, up to a distance of 20 km to the nearest updraft, $h_u - h_e$ is smaller when convection is aggregated. When calculating h_e by averaging, for every updraft grid point, over all nonupdraft grid points within a given neighborhood, the results are weighted strongly toward values close to the updrafts. This explains why $h_u - h_e$ remains smaller for aggregated convection, even if a 50 km neighborhood is considered (closed circles in Figure 4). In a 10 km neighborhood, the difference between h_u and h_e is only half as large for aggregated as for unaggregated convection (Figure 4). An air parcel close to aggregated convective updrafts does not only have high values of moist static energy but also has high values of radioactive tracer concentration, showing that the high moist static energy can be explained with the air parcels history: it got rather recently detrained from one of the nearby updrafts (Figure 1). As the differences in h_e reflect changes in $q_{v,e}$ (Figure 4), aggregated convective updrafts can be thought of as protecting themselves from the dry domain-mean environment by creating a moist shell.

Because aggregated convective updrafts are surrounded by a moist shell, the same amount of entrained air causes less cloud water to evaporate and to cool the updraft (compared to unaggregated convection). Thus, in case of aggregated convection, entrainment is less efficient in reducing updraft buoyancy—even though the bulk entrainment rate is higher. As the moist shell cannot be resolved by current GCMs and is not parameterized by convection schemes, this effect is missing in GCMs.

4. Conclusions

In this study, we analyze how bulk entrainment depends on convective aggregation. For this purpose, we use convection-permitting simulations in a nonrotating RCE framework. A 1 km grid is chosen to estimate

bulk entrainment rates for deep convection with a “radioactive tracer”, set to 1 at the surface and decaying in the atmosphere with an e -folding time scale of 4 days. Against our initial expectation, we find that the bulk entrainment rate does not decrease with convective aggregation but increases. Though updraft size and static stability increase, these effects are overcompensated by changes in resolved horizontal turbulence kinetic energy (Υ). Υ is much higher in the close environment of updraft grid points in case of aggregated convection, which we suspect is a consequence of the closer packing of aggregated updrafts. However, as aggregated updrafts are surrounded by a moist shell, the moister nearby environment wins over the higher entrainment rate, and therefore, aggregated updrafts experience less buoyancy reduction through entrainment.

Beyond our RCE study, further work will be needed to explore whether an increase of entrainment rate with aggregation can be reproduced in more realistic setups and to what extent the findings depend on the form of aggregation. For example, the storm-resolving simulations over the tropical Atlantic by Klocke et al. (2017) provide an interesting model framework to answer these questions.

Our results imply that, in order to represent the effect of aggregation in a convective parameterization, as suggested by Mapes and Neale (2011) and Tobin et al. (2013), it is not consistent with the involved physical processes to decrease the entrainment rate. Instead, the environment should be adapted. In case of aggregated convection, it is not valid to assume that the properties of the entrained air, especially specific humidity, are well represented by the mean value in the GCM grid cell. Instead, a value that is closer to the value in the updraft should be used. This differentiation between the convective and large-scale environment, the moist shell, thus emerges in our simulations as a fundamental ingredient of convective organization and should be parameterized in convective parameterizations that wish to represent organization.

Acknowledgments

This research was supported by the Max Planck Society for the Advancement of Science. Computing resources were provided by the German Climate Computing Center (DKRZ), Hamburg. Primary data and scripts used in the analysis and other supplementary information that may be useful in reproducing the author's work are archived by the Max Planck Institute for Meteorology and can be obtained by contacting publications@mpimet.mpg.de. The authors thank the internal reviewer Nicolas Rochetin for his thoughtful and helpful comments.

References

- Arnold, N. P., & Randall, D. A. (2015). Global-scale convective aggregation: Implications for the MJO. *Journal of Advances in Modeling Earth Systems*, 7(4), 1499–1518. <https://doi.org/10.1002/2015MS000498>
- Becker, T., Stevens, B., & Hohenegger, C. (2017). Imprint of the convective parameterization and sea-surface temperature on large-scale convective self-aggregation. *Journal of Advances in Modeling Earth Systems*, 9(2), 1488–1505. <https://doi.org/10.1002/2016MS000865>
- Betts, A. K. (1975). Parametric interpretation of trade-wind cumulus budget studies. *Journal of the Atmospheric Sciences*, 32(10), 1934–1945. [https://doi.org/10.1175/1520-0469\(1975\)032<1934:PIOTWC>2.0.CO;2](https://doi.org/10.1175/1520-0469(1975)032<1934:PIOTWC>2.0.CO;2)
- Bretherton, C. S., Blossey, P. N., & Khairoutdinov, M. F. (2005). An energy-balance analysis of deep convective self-aggregation above uniform SST. *Journal of the Atmospheric Sciences*, 62(12), 4273–4292. <https://doi.org/10.1175/JAS3614.1>
- Bryan, G. H., Wyngaard, J. C., & Fritsch, J. M. (2003). Resolution requirements for the simulation of deep moist convection. *Monthly Weather Review*, 131(10), 2394–2416. [https://doi.org/10.1175/1520-0493\(2003\)131<2394:RRFTSO>2.0.CO;2](https://doi.org/10.1175/1520-0493(2003)131<2394:RRFTSO>2.0.CO;2)
- Couvreux, F., Hourdin, F., & Rio, C. (2010). Resolved versus parameterized boundary-layer plumes. Part I: A parametrization-oriented conditional sampling in large-eddy simulations. *Boundary-Layer Meteorology*, 134(3), 441–458. <https://doi.org/10.1007/s10546-009-9456-5>
- de Rooy, W. C., Bechtold, P., Fröhlich, K., Hohenegger, C., Jonker, H., Mironov, D., ... Yano, J.-I. (2013). Entrainment and detrainment in cumulus convection: An overview. *Quarterly Journal of the Royal Meteorological Society*, 139(670), 1–19. <https://doi.org/10.1002/qj.1959>
- Dipankar, A., Stevens, B., Heinze, R., Moseley, C., Zängl, G., Giorgetta, M., & Brdar, S. (2015). Large eddy simulation using the general circulation model ICON. *Journal of Advances in Modeling Earth Systems*, 7(3), 963–986. <https://doi.org/10.1002/2015MS000431>
- Esbensen, S. (1978). Bulk thermodynamic effects and properties of small tropical cumuli. *Journal of the Atmospheric Sciences*, 35(5), 826–837. [https://doi.org/10.1175/1520-0469\(1978\)035<0826:BTEAPO>2.0.CO;2](https://doi.org/10.1175/1520-0469(1978)035<0826:BTEAPO>2.0.CO;2)
- Feng, Z., Hagos, S., Rowe, A. K., Burleyson, C. D., Martini, M. N., & de Szoeke, S. P. (2015). Mechanisms of convective cloud organization by cold pools over tropical warm ocean during the AMIE/DYNAMO field campaign. *Journal of Advances in Modeling Earth Systems*, 7(2), 357–381. <https://doi.org/10.1002/2014MS000384>
- Heinze, R., Dipankar, A., Henken, C. C., Moseley, C., Sourdeval, O., Trömel, S., ... Quaas, J. (2017). Large-eddy simulations over Germany using ICON: A comprehensive evaluation. *Quarterly Journal of the Royal Meteorological Society*, 143(702), 69–100. <https://doi.org/10.1002/qj.2947>
- Hohenegger, C., & Bretherton, C. S. (2011). Simulating deep convection with a shallow convection scheme. *Atmospheric Chemistry and Physics*, 11(20), 10389–10406. <https://doi.org/10.5194/acp-11-10389-2011>
- Hohenegger, C., & Stevens, B. (2016). Coupled radiative convective equilibrium simulations with explicit and parameterized convection. *Journal of Advances in Modeling Earth Systems*, 8(3), 1468–1482. <https://doi.org/10.1002/2016MS000666>
- Khairoutdinov, M., & Randall, D. (2006). High-resolution simulation of shallow-to-deep convection transition over land. *Journal of the Atmospheric Sciences*, 63(12), 3421–3436. <https://doi.org/10.1175/JAS3810.1>
- Klocke, D., Pincus, R., & Quaas, J. (2011). On constraining estimates of climate sensitivity with present-day observations through model weighting. *Journal of Climate*, 24(23), 6092–6099. <https://doi.org/10.1175/2011JCLI4193.1>
- Klocke, D., Brueck, M., Hohenegger, C., & Stevens, B. (2017). Rediscovery of the doldrums in storm-resolving simulations over the tropical Atlantic. *Nature Geoscience*, 10(12), 891–896. <https://doi.org/10.1038/s41561-017-0005-4>
- Knight, C. G., Knight, S. H. E., Massey, N., Aina, T., Christensen, C., & Frame, D. J. (2007). Association of parameter, software, and hardware variation with large-scale behavior across 57,000 climate models. *Proceedings of the National Academy of Sciences of the United States of America*, 104(30), 12,259–12,264. <https://doi.org/10.1073/pnas.0608144104>
- Kuang, Z., & Bretherton, C. S. (2006). A mass-flux scheme view of a high-resolution simulation of a transition from shallow to deep cumulus convection. *Journal of the Atmospheric Sciences*, 63(7), 1895–1909. <https://doi.org/10.1175/JAS3723.1>
- Lilly, D. K. (1962). On the numerical simulation of buoyant convection. *Tellus*, 14(2), 148–172. <https://doi.org/10.1111/j.2153-3490.1962.tb00128.x>

- Lu, C., Liu, Y., Zhang, G. J., Wu, X., Endo, S., Cao, L., ... Guo, X. (2016). Improving parameterization of entrainment rate for shallow convection with aircraft measurements and large-eddy simulation. *Journal of the Atmospheric Sciences*, 73(2), 761–773. <https://doi.org/10.1175/JAS-D-15-0050.1>
- Mapes, B., & Neale, R. (2011). Parameterizing convective organization to escape the entrainment dilemma. *Journal of Advances in Modeling Earth Systems*, 3(2), M06004. <https://doi.org/10.1029/2011MS000042>
- Mlawer, E. J., Taubman, S. J., Brown, P. D., Iacono, M. J., & Clough, S. A. (1997). Radiative transfer for inhomogeneous atmospheres: RRTM, a validated correlated-k model for the longwave. *Journal of Geophysical Research*, 102(D14), 16,663–16,682. <https://doi.org/10.1029/97JD00237>
- Morton, B. R., Taylor, G., & Turner, J. S. (1916). Turbulent gravitational convection from maintained and instantaneous sources. *Proceedings of the Royal Society of London A: Mathematical, Physical and Engineering Sciences*, 234, 1–23. <https://doi.org/10.1098/rspa.1956.0011>
- Muller, C. J., & Bony, S. (2015). What favors convective aggregation and why? *Geophysical Research Letters*, 42, 5626–5634. <https://doi.org/10.1002/2015GL064260>
- Queslati, B., & Bellon, G. (2013). Convective entrainment and large-scale organization of tropical precipitation: Sensitivity of the CNRM-CM5 hierarchy of models. *Journal of Climate*, 26(9), 2931–2946. <https://doi.org/10.1175/JCLI-D-12-00314.1>
- Romps, D. M. (2010). A direct measure of entrainment. *Journal of the Atmospheric Sciences*, 67(6), 1908–1927. <https://doi.org/10.1175/2010JAS3371.1>
- Romps, D. M., & Kuang, Z. (2011). A transilient matrix for moist convection. *Journal of the Atmospheric Sciences*, 68(9), 2009–2025. <https://doi.org/10.1175/2011JAS3712.1>
- Seifert, A., & Beheng, K. D. (2006). A two-moment cloud microphysics parameterization for mixed-phase clouds. Part 1: Model description. *Meteorology and Atmospheric Physics*, 92(1), 45–66. <https://doi.org/10.1007/s00703-005-0112-4>
- Sherwood, S. C., Bony, S., & Dufresne, J.-L. (2014). Spread in model climate sensitivity traced to atmospheric convective mixing. *Nature*, 505(7481), 37–42. <https://doi.org/10.1038/nature12829>
- Siebesma, A. P., & Cuijpers, J. W. M. (1995). Evaluation of parametric assumptions for shallow cumulus convection. *Journal of the Atmospheric Sciences*, 52(6), 650–666. [https://doi.org/10.1175/1520-0469\(1995\)052<0650:EOPAF5>2.0.CO;2](https://doi.org/10.1175/1520-0469(1995)052<0650:EOPAF5>2.0.CO;2)
- Siebesma, A. P., Bretherton, C. S., Brown, A., Chlond, A., Cuxart, J., Duynkerke, P. G., ... Stevens, D. E. (2003). A large eddy simulation intercomparison study of shallow cumulus convection. *Journal of the Atmospheric Sciences*, 60(10), 1201–1219. [https://doi.org/10.1175/1520-0469\(2003\)60<1201:ALESIS>2.0.CO;2](https://doi.org/10.1175/1520-0469(2003)60<1201:ALESIS>2.0.CO;2)
- Siebesma, A. P. (1996). On the mass flux approach for atmospheric convection, *Workshop on New Insights and Approaches to Convective Parametrization* (pp. 25–57). Reading, United Kingdom: ECMWF.
- Tobin, I., Bony, S., Holloway, C. E., Grandpeix, J.-Y., Sèze, G., Coppin, D., ... Roca, R. (2013). Does convective aggregation need to be represented in cumulus parameterizations? *Journal of Advances in Modeling Earth Systems*, 5(4), 692–703. <https://doi.org/10.1002/jame.20047>
- Tomassini, L., Voigt, A., & Stevens, B. (2015). On the connection between tropical circulation, convective mixing, and climate sensitivity. *Quarterly Journal of the Royal Meteorological Society*, 141(689), 1404–1416. <https://doi.org/10.1002/qj.2450>
- Tompkins, A. M., & Craig, G. C. (1998). Radiative-convective equilibrium in a three-dimensional cloud-ensemble model. *Quarterly Journal of the Royal Meteorological Society*, 124(550), 2073–2097. <https://doi.org/10.1002/qj.49712455013>
- Tompkins, A. M., & Semie, A. G. (2017). Organization of tropical convection in low vertical wind shears: Role of updraft entrainment. *Journal of Advances in Modeling Earth Systems*, 9, 1046–1068. <https://doi.org/10.1002/2016MS000802>
- Turner, J. S. (1963). The motion of buoyant elements in turbulent surroundings. *Journal of Fluid Mechanics*, 16(1), 1–16. <https://doi.org/10.1017/S0022112063000549>
- Yanai, M., Esbensen, S., & Chu, J.-H. (1973). Determination of bulk properties of tropical cloud clusters from large-scale heat and moisture budgets. *Journal of the Atmospheric Sciences*, 30(4), 611–627. [https://doi.org/10.1175/1520-0469\(1973\)030<0611:DOBPOT>2.0.CO;2](https://doi.org/10.1175/1520-0469(1973)030<0611:DOBPOT>2.0.CO;2)
- Zängl, G., Reinert, D., Rípodas, P., & Baldauf, M. (2015). The ICON (ICOsaedral Non-hydrostatic) modelling framework of DWD and MPI-M: Description of the non-hydrostatic dynamical core. *Quarterly Journal of the Royal Meteorological Society*, 141(687), 563–579. <https://doi.org/10.1002/qj.2378>
- Zhang, G. J., Wu, X., Zeng, X., & Mitovski, T. (2016). Estimation of convective entrainment properties from a cloud-resolving model simulation during TWP-ICE. *Climate Dynamics*, 47(7), 2177–2192. <https://doi.org/10.1007/s00382-015-2957-7>